Molecule fluorescence modified by a slit-based nanoantenna with dual gratings

Hongming Shen, Guowei Lu,* Tianyue Zhang, Jie Liu, Yingbo He, Yuwei Wang, and Qihuang Gong

State Key Laboratory for Mesoscopic Physics, Department of Physics, Peking University, Beijing 100871, China
**Corresponding author: guowei.lu@pku.edu.cn*

Received March 5, 2013; revised July 14, 2013; accepted July 25, 2013;
posted July 30, 2013 (Doc. ID 186395); published August 20, 2013

In this study, molecule fluorescence modified by slit-based nanoantennas surrounded with metal gratings was investigated by employing the finite-difference time-domain method. We quantified the relative contribution of excitation and emission gains to the total fluorescence enhancement. The simulation results show that the asymmetric dual-grating (DG) antenna provides an efficient way to control the local excitation enhancement, the collection efficiency, and the quantum efficiency separately for bright emission and beaming light. We also investigated the dependence of fluorescence enhancement on the geometric parameters of the antenna, such as the nano-slit width and number of grooves. The asymmetric DG structure greatly improves the flexibility of the nanostructure design to further optimize the plasmonic enhancement effect and provides a promising route to manipulate single-molecule fluorescence emission.

OCIS codes: (020.0020) Atomic and molecular physics; (050.0050) Diffraction and gratings; (250.5403) Plasmonics; (300.6280) Spectroscopy, fluorescence and luminescence.
http://dx.doi.org/10.1364/JOSAB.30.002420

1. INTRODUCTION

Efficiently modulating spontaneous emission of single molecules or quantum dots holds great promise for a wide range of fluorescence-based applications, including fluorescence imaging [1], DNA sequencing [2], molecular sensing [3], and photonic integration devices [4,5]. So far, a growing number of resonant structures, such as hyperbolic metamaterials [6], photonic crystal microcavities [7], and optical antennas, have been studied to modify the fluorescence emission process. Of these, optical antennas based on metallic nanostructures provide an efficient way to concentrate light into a nanoscale volume to overcome the detection limit due to the diffraction effect [8–10]. Importantly, various types of optical antennas, from a single particle to arrays of apertures, have also been reported to tailor the excitation and emission processes [11,12], e.g., tune the luminescence spectrum [13,14], modify the decay lifetime [15,16], and control the radiation directivity [17–19]. Recently, nanoapertures surrounded by periodic corrugations [20] have gained significant popularity for their unique ability to improve the fluorescence intensity and simultaneously provide directional control on the emission. As we know, both the fluorescence enhancement factor and directivity are key elements for the detection of a single molecule.

In the past decades, extensive work has been done to reveal the physical origins of extraordinary transmission properties [21–23] and beaming effects [24,25] of the slit (or hole)-groove antennas. Recently, people begin to focus on modulating the molecule fluorescence by taking advantage of these structures. Aouani *et al.* first reported that a fluorescence enhancement factor of up to 120-fold with a narrow beam of $\pm 15°$ could be experimentally observed using a nanoaperture surrounded by 5 grooves [26]. Jun and colleagues presented that the grating structure can be engineered to produce plasmonic beaming and active control over fluorescent emission [27]. Several studies have also been carried out to explore the dependence of fluorescence properties on antenna geometric parameters [28,29]. However, the goals to get a much larger enhancement factor and more tunable directional control still remain an open challenge. To optimize both parameters requires a sufficiently broad resonant peak of the nanoantennas or a small Stokes shift between the laser excitation and the fluorescence emission. This makes it inconvenient to design the grating structure and restricts the fluorescence enhancement factor to some extent with the single-grating (SG) structure, in which the plasmonic grating acts as both an input surface and an output surface. An elegant way to provide resonant conditions at two different wavelengths could be realized by introducing an asymmetric dual-grating (DG) structure, which has been applied successfully for optical transmission [30–32]. Such asymmetric structures enable us to overcome the aforementioned problem in engineering molecule fluorescence process.

In this study, we theoretically explore the fluorescence characteristics in a subwavelength slit surrounded by asymmetric metal gratings on both sides of a thick gold film. We separate significant contributions of the excitation and emission gains from the overall fluorescence enhancement. Simulation results confirm that the metallic gratings play a crucial role in the fluorescence enhancement process. Compared to the SG antenna, the DG structure offers higher fluorescence enhancement and better flexibility to control the emission's angular distribution. Our discussion gives an instructive insight into the plasmonic-enhanced fluorescence process based on the slit–groove structure and the results are in good agreement with the previously reported experimental studies.

2. SIMULATION MODEL

Figure 1 shows a schematic of the metal antenna structures used in this study. We compare three cases: (a) a bare slit without side grooves, (b) a SG structure with grooves patterned on the bottom side, and (c) a DG structure with asymmetrical grooves on both sides of the metal film. Gold was chosen as the antenna material and its dielectric constant was taken from [33] and fitted by the Drude–Lorentz dispersion model. The upper half-space, as well as the slit cavity, is filled with water, whereas the substrate medium is considered to be silica. In the excitation process, the structures are under normal incidence illumination with plane waves at a wavelength of 633 nm (with the electric field polarizing in that x direction called "TM polarization" here). In contrast to the other two cases, the DG structure is illuminated from the upper side. In the emission process, we assumed an oriented dipole source ($\lambda_{em} = 670$ nm) positioned at the slit center, which corresponds to the maximum emission peak of the widely used Cyanine 5 (Cy5) dye molecule. The simulations were carried out by employing the 2D finite-difference time-domain (FDTD) method, which has been extensively tested and applied in the calculation of plasmonic nanostructures [34]. We apply the perfect matched layer (PML) absorption boundary conditions and the mesh pitch is 1 nm (unless otherwise stated). Many attempts have been made to optimize the DG antenna for a large enhancement factor and narrow directivity. Finally, optimized geometric parameters for our simulations are obtained as follows. For the upper-side interface, we set the groove periodicity $G_2 = g_2 = 380$ nm, depth $d_2 = 30$ nm, and width $a_2 = 190$ nm. We choose $G_1 = g_1 = 440$ nm, $d_1 = 60$ nm, and $a_1 = 220$ nm for the bottom-side interface, as indicated in Fig. 1. These dimensional scales are typical parameters in the reported experimental studies [26,28]. For comparison, the bottom-side grooves of the SG and DG antennas have identical parameters. In all cases, we took the slit thickness $H = 240$ nm, width $W = 80$ nm, and the number of grooves $N = 6$.

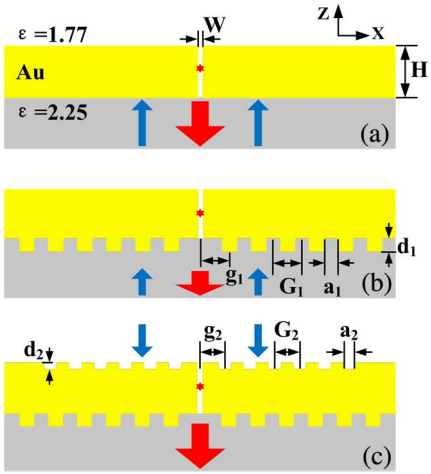

Fig. 1. Schematics of three types of plasmonic antennas studied in our simulations: (a) a bare slit without gratings, (b) a SG structure and (c) an asymmetric DG structure. The structures are illuminated with p-polarized planar continuous light under normal incidence at 633 nm. A dipole emitter with emission wavelength of 670 nm is placed at the center of the slit (oriented in the x direction). The geometric parameters that require careful optimization are defined in the figure and detailed in the text. In our 2D geometry, the slit length L is infinite.

3. RESULTS AND DISCUSSION

As we known, the fluorescence process can be theoretically separated into two independent steps: excitation and emission. Thus, the fluorescence enhancement factor η_F can be expressed approximately as $\eta_F \propto \eta_{exc}\eta_\phi\eta_k$ [9,35,36], where the factor $\eta_{exc} = |E|^2/|E_0|^2$ represents a local field enhancement to quantify the excitation gain. The quantities $|E|^2$ and $|E_0|^2$ are the electrical field intensities with and without plasmonic antennas, respectively. The product of quantum efficiency enhancement $\eta_\phi = \eta/\eta_0$ and collection efficiency enhancement $\eta_k = \kappa/\kappa_0$ are responsible for the emission gain. The quantities η and κ stand for the quantum efficiency modified by the plasmonic antenna and the collection efficiency relative to the setup. Based on Poynting's theory [37], we then estimate the contributions of excitation and emission gains to the total fluorescence enhancement. Basically, the extraordinary transmission mechanism of the aperture–groove antennas is separated into three processes: couple in, transmit through, and couple out. These processes can also be found in the plasmonic modified fluorescence process, and more detail will be discussed in the following. It should be noted that the side grooves play different roles in the excitation and emission processes. Due to weak interaction between the input and output surfaces, the asymmetrical DG structure offers an efficient way to control the excitation and emission processes separately.

To explore how the fluorescence process is modified by the corrugated subwavelength slit, we began by calculating the local field enhancement η_{exc} in the excitation process. Time-averaged electrical field distributions $|E|^2$ in the vicinity of the slit were calculated for three cases: a bare slit, a SG structure, and a DG structure, as shown in Figs. 2(a)–2(c), respectively. We observed large field intensities localized inside the DG structure. To give an intuitive view, the corresponding local excitation enhancement η_{exc} normalized by the incident intensity $|E_0|^2$ along $X = 0$ and $Z = 0$ are also depicted in Figs. 2(d) and 2(e). For a bare slit, light cannot efficiently excite surface plasmon polaritons (SPPs) so that the factor η_{exc} at the slit center is only 2.6-fold. For a SG structure, the resonant wavelength of the bottom-side grooves is ~650 nm, taking a trade-off between the laser excitation and emission wavelength into account. Hence, the factor η_{exc} can be slightly enhanced to 5.3, which is in agreement with experiment results reported in [26]. As we know, the metal gratings here serve as an input surface and provide the necessary momentum to match SPPs mode. However, only frequencies in a narrow band could effectively couple free propagating light to the SPPs for a given metal grating [20]. For the DG structure, the factor η_{exc} comes to 50.4, which is about 10-fold higher than that of the SG structure. We ascribe this to the following reasons. First, the resonant wavelength is tuned to ~637 nm by optimizing the geometrical parameters of the upper-side grooves, which is almost consistent with the excitation light (633 nm). This greatly improves the coupling efficiency of the laser excitation to the metal gratings. Second, we tune the slit parameters (H, W) to further optimize the excitation enhancement factor because of the constructive coupling between the slit cavity mode and the induced SPP resonance [38–40]. As we know, both the change of slit width W and slit thickness H would tune the cavity resonances [41,42]. The maximum field enhancement can be

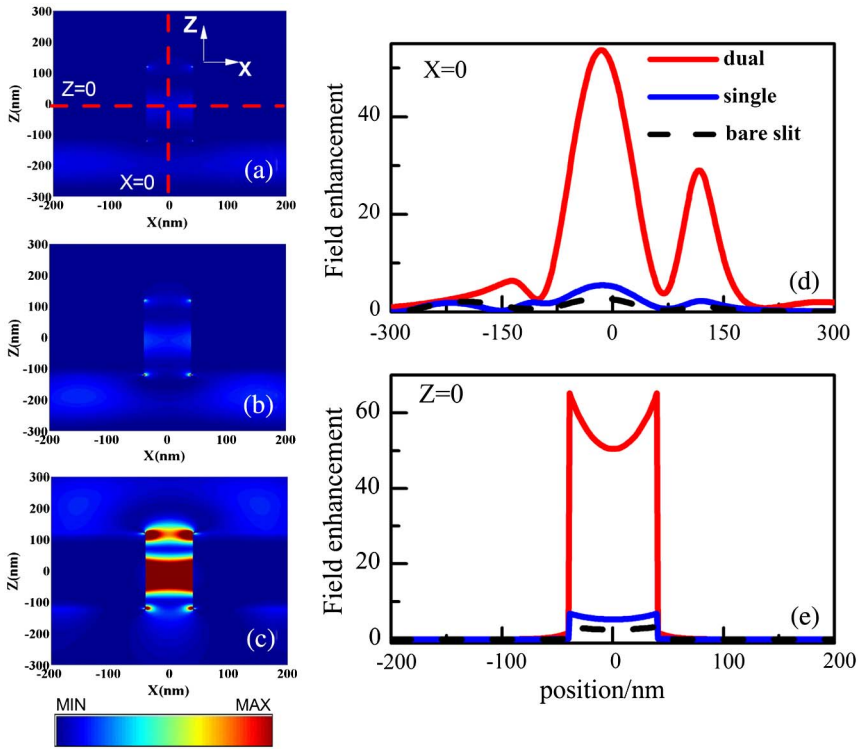

Fig. 2. Time-averaged field distributions $|E|^2$ in the vicinity of the slit for the three metallic antennas: (a) a bare slit, (b) a SG and (c) a DG. Corresponding field enhancement factors normalized to the initial field $|E_0|^2$ along (d) $X = 0$ and (e) $Z = 0$ in the X–Z plane are also plotted. The structures are under normal incidence illumination with p-polarized plane wave at 633 nm.

expected when the resonance of the slit cavity matches the resonance of the plasmon surface wave.

Next we calculated the far-field radiation patterns to quantify the collection efficiency enhancement η_k in the emission process, as presented in Fig. 3(a). To give an intuitive view, the normalized angular radiation patterns in all directions were also plotted in a polar diagram (inset) for three cases: a SG structure (red line), free solution without an antenna (blue line), and emission from air (black line). Here, a dipole source ($\lambda_{em} = 670$ nm) orienting in the x direction was placed at the slit center. We first recorded the near-field data [$E(t)$, $H(t)$] of a line with width of 14 μm located 350 nm beneath the metal/silica interface. Then, a 2D near-to-far-field (NTFF) transformation method was performed to calculate the angular radiation power density $P(\theta)$, which has been carefully tested by 3D calculations (not shown here) and is well consistent with the experiment results [27,43,44]. The directivity is a quantity from antenna theory that characterizes the ability of antenna of beaming light and is defined as $D(\theta) = \pi P(\theta)/\int P(\theta)\mathrm{d}\theta$. Here, we defined the collection efficiency as $\kappa = P_{col}/P_{rad}$, where P_{col} is the power density collected by a lens (for example, a 0.5 NA water immersion objective with a maximum detectable angle of ±22°) and P_{rad} is the total power density radiated to the lower half-space. By calculating the collection efficiency $\kappa = \int_{-22°}^{+22°} P(\theta)\mathrm{d}\theta / \int_{-90°}^{+90°} P(\theta)\mathrm{d}\theta$, we finally quantified the collection efficiency enhancement as $\eta_k = \kappa/\kappa_0$, where κ_0 represents the collection efficiency in free solution. For comparison, we also calculated the radiation pattern of a single dipole in free solution [gray dashed line in Fig. 3(a)]. In the case of a bare slit, the dipole emission diffracts in all directions (black line), which reduces the collection efficiency enhancement η_k to 0.66 (with respecte to the free solution). Interestingly, for the

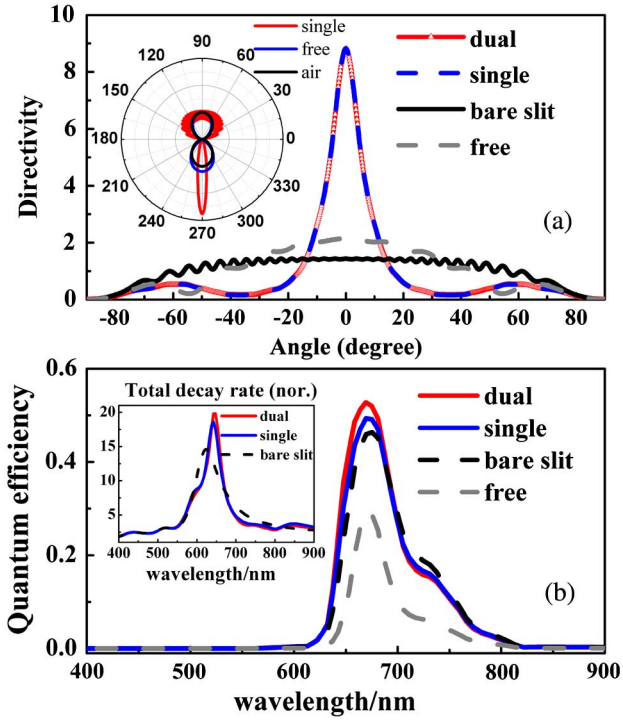

Fig. 3. (a) Calculated far-field angular distributions in the X–Z plane based on the NTFF method. Inset: normalized angular radiation patterns of a dipole emission in all directions for three cases: a SG structure (red line), free solution without antenna (blue line), and emission from air (black line). An electrical dipole emitter ($\lambda_{em} = 670$ nm), oriented in the x direction, was placed at the slit center. Note that the emissions to the bottom side are calculated and compared for the three structures. (b) Modified quantum efficiency and total decay rate (inset) as functions of wavelength are plotted for different plasmonic structures.

SG (blue dashed line) and DG (red line) structures, we observe both collimated beams normal to the metal surface with a half-width at half-maximum of ±6° and the collection efficiency enhancements are up to ~1.5-fold. The angular distributions act quite similar due to the identical bottom-side metal gratings. It is obvious from Fig. 3(a) that the interaction between the upper-side and bottom-side interfaces is weak for a thick gold film. Whether the upper-side interface is corrugated or not, the beaming light effect is mainly determined by the output gratings (i.e., bottom-side interface).

In order to further understand the modification of decay rate and quantum yield in the emission process, Fig. 3(b) shows the modified quantum efficiency η as a function of wavelength for a dipole placed at the slit center. It should be pointed out that the quantum efficiency is different when the dipole is placed at different positions inside the slit cavity. Nevertheless, the modified quantum efficiency can be expressed as $\eta(\omega) = \eta_0(\omega)/\{[(1-\eta_0(\omega)]/F(\omega) + \eta_0(\omega)/\eta_a(\omega)\}$ [45,46], where η_0 is the original quantum efficiency in free solution, F is the Purcell factor, and η_a is the antenna efficiency. For comparison, we presented a normalized spectrum of Cy5 dye in free solution (gray dashed line). As we can see, the quantum efficiency enhancement η_φ at an emission wavelength of 670 nm is almost the same for a bare slit (~1.61), the SG structure (~1.73), and the DG structure (~1.85). Note that the intrinsic quantum efficiency η_0 at 670 nm is set to be 0.3. Additionally, we performed a simulation on the total decay rate Γ_{tot} as a function of wavelength [inset of Fig. 3(b)], which represents all the energy emitted by a dipole. As we know, the increase in the total decay rate corresponds to the reduction of fluorescence lifetime. Here again, the decay rates for the three structures are similar, especially at a wavelength of 670 nm. The simulation results stand in good agreement with the notion that the slit cavity determines mainly the decay lifetime and the quantum efficiency, while the effect of the upper-side or bottom-side grooves on the fluorescent lifetime is confirmed to be negligible [26,27].

Table 1 summarizes the relative contributions of the excitation and emission gains to the total fluorescence enhancement. The results show that significant fluorescence enhancement up to 140-fold can be realized with the DG structure, which is nearly 10-fold higher than the SG structure and 50-fold higher than the bare slit structure. We ascribe it to the excellent local excitation gain achieved by introducing the asymmetrical upper-side grooves. The input corrugations contribute primarily to a large local excitation gain in the excitation process. It is convenient to design the input gratings based on different laser excitations. Active beaming control (on-axis or off-axis) and narrow directionality could also be achieved by carefully tuning the geometrical parameters of the output corrugations. It should be pointed out that the different output patterns make little impact on the local excitation gain of the input surface. In order to make clear the advantages of the DG structure, we also explore how the geometric parameters, i.e., groove number N (Fig. 4) and slit-to-first-groove distance g (Fig. 5), affect strongly the fluorescence process. The results in Fig. 4 indicate that a certain number of grooves ($N = 8$) leads to saturation of the local field enhancement factor in the excitation process. Interestingly, the emission collection efficiencies show little difference with the increase of N compared to the bare slit structure. Even a single groove ($N = 1$) is sufficient to produce a collimated beam. We also find g is crucial to control the traveling phase of SPPs to the slit cavity to realize constructive or destructive interference [47] in the excitation and emission process. As shown in Fig. 5(a), we can adjust the distance g_2 on the upper side of the DG antenna to realize light transmission enhancement and suppression in the excitation process. However, Fig. 5(b) confirms that the slit-to-first-groove distance g plays an important part in the far-field angular pattern, which explains why only a single groove can realize high collection efficiency. We thus can also tune the parameter g_1 on the bottom side of the DG antenna to obtain active directional control.

Last, we are interested in the dependence of fluorescence enhancement on the slit width **W**, as depicted in Fig. 6. With the slit width increasing from 40 to 180 nm, we observe the local field enhancement factors in Fig. 6(a) increase first and then decrease for the three cases. The optimal slit width for the DG structure is 80 nm compared to 60 nm for the SG structure and the bare slit structure. It should be noted that the slit cavity mode would be changed when increasing the slit width **W**, leading to a shift of the resonance. The optimal field enhancement factor is obtained only when the resonances of the SPPs and the slit cavity are consistent with each other. In the emission process, the quantum efficiency enhancements [Fig. 6(b)] quickly increase with the decrease of slit width W and then rise to a maximum when W is equal to 60 nm, but decrease when further reducing the slit width. As to the total decay rate [inset of Fig. 6(b)], it can be seen that all curves have a similar shape: falling fast with the increasing of slit width. In other words, the fluorescence lifetimes are

Table 1. Relative Contribution of Excitation and Emission Gains to the Overall Fluorescence Enhancement Based on Different Metal Structures

	η_{exc}	η_k	η_ϕ	η_F
Bare slit	2.6	0.66	1.61	2.8
SG structure	5.3	1.50	1.73	13.7
DG structure	50.4	1.50	1.85	139.7

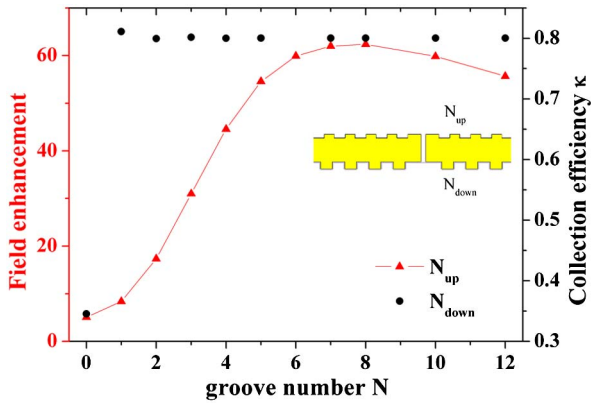

Fig. 4. Local field enhancement η_{exc}(red) at the slit center and collection efficiency κ (black) as functions of groove number N corrugated on the upper-side and bottom-side of the DG antenna. The mesh pitch here is set to be 2 nm.

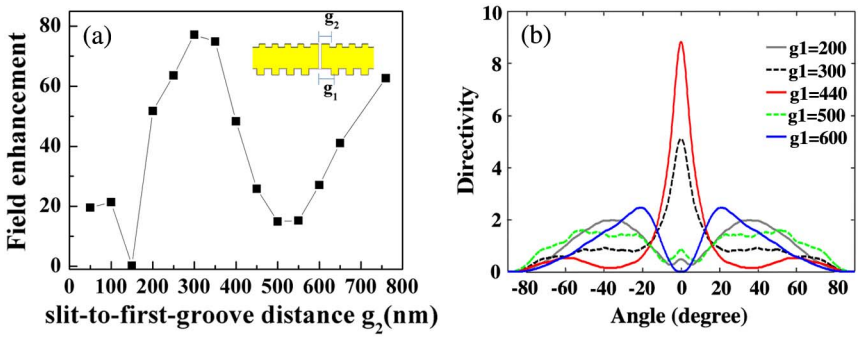

Fig. 5. Dependence of fluorescence characteristics on the slit-to-first-groove distance g for the DG antenna. The illumination wavelength is 633 nm. As we can see, the factor of local field enhancement (a) at the slit center changes in the form of oscillation as the increase of distance g_2. (b) Far-field directivities of a single dipole source ($\lambda = 670$ nm) inside the center of the slit cavity. We observe beaming or splitting light for g_1 ranging from 200 to 600 nm. The mesh pitch here is 2 nm.

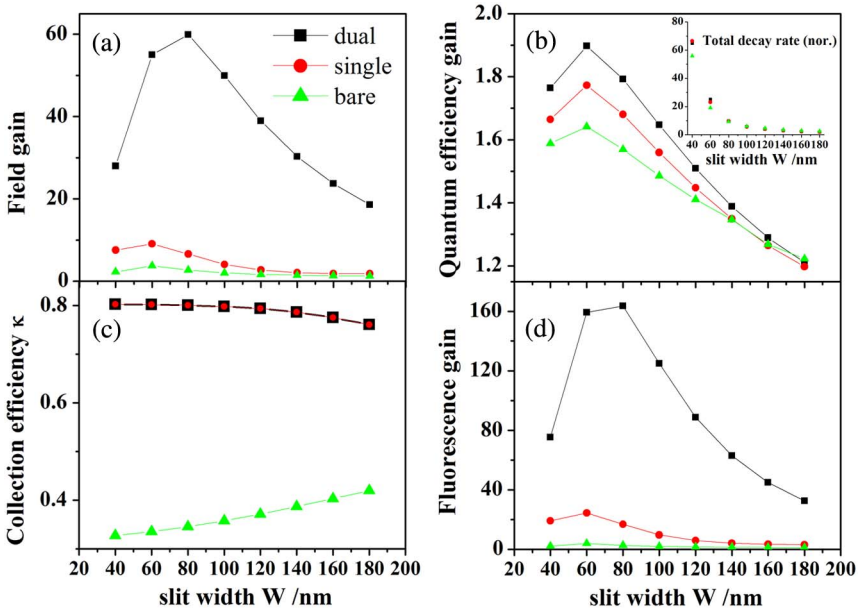

Fig. 6. Dependence of fluorescence enhancement on the slit width W of the three antenna structures. (a) Field enhancement at the slit center under illumination of 633 nm. (b) Quantum efficiency gain and normalized total decay rate (inset) for a dipole placed at the slit center with 670 nm. (c) Collection efficiency (noted that the curve for the SG structure overlaps with the curve for the DG structure here) and (d) total fluorescence enhancement as functions of slit width. The mesh pitch here is set to be 2 nm.

shortened as the mode volume of the slit cavity is decreased [48]. It is confirmed again that the decay lifetime is mainly determined by the slit cavity and has little to do with the groove structure. Additionally, the effect of slit width on collection efficiency κ turns out to be small for both the DG and SG structures, as depicted in Fig. 6(c). We observe only a slight decrease of the collection efficiency when increasing the slit width because the beam radiation pattern is controlled mainly by the groove structure. However, for the bare slit structure, the collection efficiency decreases with the decrease of slit width due to a serious diffraction effect for a small slit width. Figure 6(d) summarizes the fluorescence gain as a function of slit width W. Similar to the local field enhancements, the overall fluorescence gain increases first and then decreases for the three antennas. It can be seen that, regardless of the slit size, the DG structure always exhibits a much higher enhancement effect than the SG and bare slit antennas.

We would like to specify that all the simulation results discussed above are performed by the 2D FDTD method and are carefully tested and compared to the 3D FDTD calculations (not shown here). Minor differences in the values between the 2D and 3D simulations may exist, but the physical laws are consistent with each other.

4. CONCLUSIONS

We theoretically investigate the fluorescence properties modified by a subwavelength slit antenna with asymmetric doubly corrugated gratings milled in a thick gold film. Our study demonstrates a detailed insight into the antenna modified fluorescence process: (i) the input corrugations are primarily contributed to local excitation enhancement, and (ii) the output corrugations are responsible for beaming light leading to high collection efficiency, (iii) while the slit cavity mainly sets the decay lifetime and quantum yield. Another remarkable point is that the interaction between the upper-side and bottom-side gratings is slight, which provides a way to control the excitation and emission processes separately. Such

asymmetrical DGs structure provides a flexible and powerful platform to manipulate the single-molecule spontaneous emission. Although additional trials are still needed to test and verify the simulation findings, our results stand in good agreement with the previous experiments and provide a promising guide for the slit–groove-antenna-based plasmonic manipulated molecule fluorescence.

ACKNOWLEDGMENTS

This work was supported by the National Key Basic Research Program of China (grant no. 2013CB328703) and the National Natural Science Foundation of China (grant nos. 61008026, 11121091, 90921008, and 91221304).

REFERENCES

1. V. Ntziachristos, "Fluorescence molecular imaging," Annu. Rev. Biomed. Eng. **8**, 1–33 (2006).
2. B. McNally, A. Singer, Z. Yu, Y. Sun, Z. Weng, and A. Meller, "Optical recognition of converted DNA nucleotides for single-molecule DNA sequencing using nanopore arrays," Nano Lett. **10**, 2237–2244 (2010).
3. X. Cui, K. Tawa, H. Hori, and J. Nishii, "Tailored plasmonic gratings for enhanced fluorescence detection and microscopic imaging," Adv. Funct. Mater. **20**, 546–553 (2010).
4. T. Pakizeh and M. Kall, "Unidirectional ultracompact optical nanoantennas," Nano Lett. **9**, 2343–2349 (2009).
5. F. Bernal Arango, A. Kwadrin, and A. F. Koenderink, "Plasmonic antennas hybridized with dielectric waveguides," ACS Nano **6**, 10156–10167 (2012).
6. J. Kim, V. P. Drachev, Z. Jacob, G. V. Naik, A. Boltasseva, E. E. Narimanov, and V. M. Shalaev, "Improving the radiative decay rate for dye molecules with hyperbolic metamaterials," Opt. Express **20**, 8100–8116 (2012).
7. P. N. Melentiev, T. V. Konstantinova, A. E. Afanasiev, A. A. Kuzin, A. S. Baturin, and V. I. Balykin, "Single nanohole and photoluminescence: nanolocalized and wavelength tunable light source," Opt. Express **20**, 19474–19483 (2012).
8. P. Mühlschlegel, H. J. Eisler, O. J. F. Martin, B. Hecht, and D. W. Pohl, "Resonant optical antennas," Science **308**, 1607–1609 (2005).
9. M. J. Levene, J. Korlach, S. W. Turner, M. Foquet, H. G. Craighead, and W. W. Webb, "Zero-mode waveguides for single-molecule analysis at high concentrations," Science **299**, 682–686 (2003).
10. P. Bharadwaj, B. Deutsch, and L. Novotny, "Optical antennas," Adv. Opt. Photon. **1**, 438–483 (2009).
11. R. Esteban, T. V. Teperik, and J. J. Greffet, "Optical patch antennas for single photon emission using surface plasmon resonances," Phys. Rev. Lett. **104**, 26802 (2010).
12. M. Yorulmaz, S. Khatua, P. Zijlstra, A. Gaiduk, and M. Orrit, "Luminescence quantum yield of single gold nanorods," Nano Lett. **12**, 4385–4391 (2012).
13. M. Ringler, A. Schwemer, M. Wunderlich, A. Nichtl, K. Kürzinger, T. A. Klar, and J. Feldmann, "Shaping emission spectra of fluorescent molecules with single plasmonic nanoresonators," Phys. Rev. Lett. **100**, 203002 (2008).
14. H. Hu, H. Duan, J. K. W. Yang, and Z. X. Shen, "Plasmon-modulated photoluminescence of individual gold nanostructures," ACS Nano **6**, 10147–10155 (2012).
15. O. L. Muskens, V. Giannini, J. A. Sánchez-Gil, and J. Gómez Rivas, "Strong enhancement of the radiative decay rate of emitters by single plasmonic nanoantennas," Nano Lett. **7**, 2871–2875 (2007).
16. P. Anger, P. Bharadwaj, and L. Novotny, "Enhancement and quenching of single-molecule fluorescence," Phys. Rev. Lett. **96**, 113002 (2006).
17. A. G. Curto, G. Volpe, T. H. Taminiau, M. P. Kreuzer, R. Quidant, and N. F. van Hulst, "Unidirectional emission of a quantum dot coupled to a nanoantenna," Science **329**, 930–933 (2010).
18. X. Chen, S. Gotzinger, and V. Sandoghdar, "99% efficiency in collecting photons from a single emitter," Opt. Lett. **36**, 3545–3547 (2011).
19. T. Shegai, V. D. Miljković, K. Bao, H. Xu, P. Nordlander, P. Johansson, and M. Kall, "Unidirectional broadband light emission from supported plasmonic nanowires," Nano Lett. **11**, 706–711 (2011).
20. H. J. Lezec, A. Degiron, E. Devaux, R. A. Linke, L. Martin-Moreno, F. J. Garcia-Vidal, and T. W. Ebbesen, "Beaming light from a subwavelength aperture," Science **297**, 820–822 (2002).
21. E. C. Kinzel, P. Srisungsitthisunti, Y. Li, A. Raman, and X. F. Xu, "Extraordinary transmission from high-gain nanoaperture antennas," Appl. Phys. Lett. **96**, 211116 (2010).
22. G. D. Aguanno, N. Mattiucci, M. J. Bloemer, D. de Ceglia, M. A. Vincenti, and A. Al, "Transmission resonances in plasmonic metallic gratings," J. Opt. Soc. Am. B **28**, 253–264 (2011).
23. L. Guangyuan, X. Feng, L. Kun, K. Alameh, and X. Anshi, "Theory, figures of merit, and design recipe of the plasmonic structure composed of a nano-slit aperture surrounded by surface corrugations," J. Lightwave Technol. **30**, 2405–2414 (2012).
24. C. Wang, C. Du, and X. Luo, "Refining the model of light diffraction from a subwavelength slit surrounded by grooves on a metallic film," Phys. Rev. B **74**, 245403 (2006).
25. H. Caglayan, I. Bulu, and E. Ozbay, "Beaming of electromagnetic waves emitted through a subwavelength annular aperture," J. Opt. Soc. Am. B **23**, 419–422 (2006).
26. H. Aouani, O. Mahboub, N. Bonod, E. Devaux, E. Popov, H. Rigneault, T. W. Ebbesen, and J. Wenger, "Bright unidirectional fluorescence emission of molecules in a nanoaperture with plasmonic corrugations," Nano Lett. **11**, 637–644 (2011).
27. Y. C. Jun, K. C. Y. Huang, and M. L. Brongersma, "Plasmonic beaming and active control over fluorescent emission," Nat. Commun. **2**, 283 (2011).
28. H. Aouani, O. Mahboub, E. Devaux, H. Rigneault, T. W. Ebbesen, and J. Wenger, "Plasmonic antennas for directional sorting of fluorescence emission," Nano Lett. **11**, 2400–2406 (2011).
29. H. Aouani, O. Mahboub, E. Devaux, H. Rigneault, T. W. Ebbesen, and J. Wenger, "Large molecular fluorescence enhancement by a nanoaperture with plasmonic corrugations," Opt. Express **19**, 13056–13062 (2011).
30. S. Cakmakyapan, A. E. Serebryannikov, H. Caglayan, and E. Ozbay, "One-way transmission through the subwavelength slit in nonsymmetric metallic gratings," Opt. Lett. **35**, 2597–2599 (2010).
31. J. Bravo-Abad, F. J. Garcia-Vidal, and L. Martin-Moreno, "Wavelength de-multiplexing properties of a single aperture flanked by periodic arrays of indentations," Photon. Nanostr. Fundam. Appl. **1**, 55–62 (2003).
32. J. Zhang and G. P. Wang, "Dual-wavelength light beaming from a metal nanoslit flanked by dielectric gratings," J. Opt. Soc. Am. B **25**, 1356–1361 (2008).
33. P. B. Johnson and R. W. Christy, "Optical constants of the noble metals," Phys. Rev. B **6**, 4370–4379 (1972).
34. A. F. Oskooi, D. Roundy, M. Ibanescu, P. Bermel, J. D. Joannopoulos, and S. G. Johnson, "Meep: a flexible free-software package for electromagnetic simulations by the FDTD method," Comput. Phys. Commun. **181**, 687–702 (2010).
35. S. Kühn, U. Håkanson, L. Rogobete, and V. Sandoghdar, "Enhancement of single-molecule fluorescence using a gold nanoparticle as an optical nanoantenna," Phys. Rev. Lett. **97**, 017402 (2006).
36. C. Girard, O. J. F. Martin, G. Lévèque, G. C. des Francs, and A. Dereux, "Generalized Bloch equations for optical interactions in confined geometries," Chem. Phys. Lett. **404**, 44–48 (2005).
37. K. C. Y. Huang, Y. C. Jun, M. Seo, and M. L. Brongersma, "Power flow from a dipole emitter near an optical antenna," Opt. Express **19**, 19084–19092 (2011).
38. C. Li, Y. Zhou, H. Wang, and F. Wang, "Wavelength squeeze of surface plasmon polariton in a subwavelength metal slit," J. Opt. Soc. Am. B **27**, 59–64 (2010).
39. F. J. García-Vidal, H. J. Lezec, T. W. Ebbesen, and L. Martín-Moreno, "Multiple paths to enhance optical transmission through a single subwavelength slit," Phys. Rev. Lett. **90**, 213901 (2003).

40. D. Crouse and P. Keshavareddy, "Role of optical and surface plasmon modes in enhanced transmission and applications," Opt. Express **13**, 7760–7771 (2005).
41. E. Popov and N. Bonod, "Physics of extraordinary transmission through subwavelength hole arrays," in *Structured Surfaces as Optical Metamaterials*, A. Maradudin, ed. (Cambridge, 2011), Chap. 1, pp. 1–27.
42. A. Krishnan, T. Thio, T. J. Kim, H. J. Lezec, T. W. Ebbesen, P. A. Wolff, J. Pendry, L. Martin-Moreno, and F. J. Garcia-Vidal, "Evanescently coupled resonance in surface plasmon enhanced transmission," Opt. Commun. **200**, 1–7 (2001).
43. A. Taflove and S. C. Hagness, *Computational Electrodynamics: The Finite-Difference Time-Domain Method*, 3rd ed. (Artech House, 2005).
44. S. Kim, S. Kim, and Y. Lee, "Vertical beaming of wavelength-scale photonic crystal resonators," Phys. Rev. B **73**, 235117 (2006).
45. V. V. Klimov, "Spontaneous emission of an atom placed near the aperture of a scanning microscope," JETP Lett. **78**, 471–475 (2003).
46. A. Kinkhabwala, Z. Yu, S. Fan, Y. Avlasevich, K. Mullen, and W. E. Moerner, "Large single-molecule fluorescence enhancements produced by a bowtie nanoantenna," Nat. Photonics **3**, 654–657 (2009).
47. G. Zheng, X. Cui, and C. Yang, "Surface-wave-enabled darkfield aperture for background suppression during weak signal detection," Proc. Natl. Acad. Sci. USA **107**, 9043–9048 (2010).
48. J. Wenger, D. Gerard, J. Dintinger, O. Mahboub, N. Bonod, E. Popov, T. W. Ebbesen, and H. Rigneault, "Emission and excitation contributions to enhanced single molecule fluorescence by gold nanometric apertures," Opt. Express **16**, 3008–3020 (2008).